



Interacting mechanism and initiation prediction of multiple cracks

Qing-qing SHEN, Qiu-hua RAO, Zhuo LI, Wei YI, Dong-liang SUN

School of Civil Engineering, Central South University, Changsha 410075, China

Received 10 January 2020; accepted 26 December 2020

Abstract: The maximum Mode I and Mode II stress intensity factors (SIFs), $K_{I,kmax}(\theta)$ and $K_{II,kmax}(\theta)$ ($0^\circ < \theta < 360^\circ$), of inclined parallel multi-crack varying with relative positions (including horizontal and vertical spacings) are calculated by the complex function and integration method to analyze their interacting mechanism and determine the strengthening and weakening zone of SIFs. The multi-crack initiation criterion is established based on the ratio of maximum tension–shear SIF to predict crack initiation angle, load, and mechanism. The results show that multi-crack always initiates in Mode I and the vertical spacing is better not to be times of half crack-length for crack-arrest, which is in good agreement with test results of the red-sandstone cube specimens with three parallel cracks under uniaxial compression. This can prove the validity of the multi-crack initiation criterion.

Key words: interaction mechanism; multi-crack initiation criterion; initiation prediction; multiple cracks; stress intensity factor

1 Introduction

In rock mass engineering, arbitrary cracks and joints existing in natural rocks usually initiate and propagate, and result in failure. Fracture failure is one of the most serious and harmful disasters. Research of multiple cracks interaction has become a hot issue and attracted more and more attention.

Currently, there are mainly two research methods for multiple cracks interaction: experimental and theoretical study. Uniaxial and biaxial compression tests have been adopted to study the effect of crack geometric parameters on stress and failure mode. Results showed that more secondary cracks occur when the vertical and horizontal spacings of double cracks are small under uniaxial compression loading [1]. The crack initiation stress is obviously lower than the peak strength when the inclined angle of double cracks with respect to the horizontal line was larger than 45° [2,3]. When the inclined angle of the five

parallel cracks is about 25° , the compressive strength reaches its minimum value [4,5]. In addition, the extension trajectory of cracks could be recorded by either naked eyes [6,7] or digital speckle correlation method (DSCM) and acoustic emission (AE) techniques [8–10] during tests. Results showed that the failure modes could be classified as five basic modes: tensile failure through the crack origin plane, tensile failure along the crack plane, shear failure along the crack plane, mixed-mode failure, and splitting failure, depending on the geometric parameters of nine equal-length parallel cracks. Also, the triaxial compression test was conducted to study the stress–strain curves of red sandstone samples with double cracks [11], but it is not convenient to observe the crack propagation process because the specimen was enclosed in a triaxial loading chamber. Due to the limit of experiments, the effects of multiple cracks geometric parameters on the initiation mechanism have not been systematically analyzed. Therefore, it's necessary to seek the theoretical method for

calculating stress intensity factor (SIF) and establishing a multi-crack fracture criterion.

Many researchers used different theoretical methods to calculate SIF of multiple cracks and study the interacting mechanism. For example, the boundary collocation method was used to calculate SIF of the single edge crack [12], the single central crack [13], and double edge cracks [14] in a finite two-dimensional plate. Complex variable method was adopted by BENTHEM and KOITER [15], and SNEDDON and LOWENGRUB [16] to solve some special multi-crack problems such as collinear, parallel, or star cracks. The pseudo-tension method is also widely applied. HORRI and NEMAT-NASSER [17,18] utilized the pseudo-tension method to calculate the SIF of double cracks and KACHANOV [19–21] simplified this method to estimate the SIF of double-crack by the superposition technique. Based on KACHANOV's method, ZHU et al [22] investigated the interaction of two offset parallel cracks with different level intervals, vertical intervals, and crack lengths and indicated three kinds of interaction: reinforcing, shielding, and null. Besides, LI et al [23] improved the accuracy of KACHANOV's method by only considering the effect of the linearly varying component (neglecting the non-uniform component). CHEUNG et al [24] adopted the Fredholm integral equation solution and weighted residual method to calculate the SIF of dual cracks. On the whole, current studies are mostly focused on the Mode I ($K_{I}(0)$) and Mode II ($K_{II}(0)$) SIFs of multiple cracks along the original crack plane. But multiple cracks do not always initiate and propagate in their original plane, e.g., the occurrence of wing cracks.

To understand the interaction mechanism of multiple cracks better, fracture criteria need to be established for predicting crack initiation. In classic fracture mechanics, there are mainly three types of mixed-mode fracture criteria: stress-based fracture criterion [25–27], strain-based fracture criterion [28], and energy-based fracture criterion [29–31], where the fracture mode (tensile or shear) is considered to be the same as the loading form. However, for brittle materials, the tensile strength is much smaller than its shear strength and thus the tensile (Mode I) fracture usually occurs even under pure shear loading. These fracture

criteria can better predict Mode I fracture under arbitrary loading conditions (pure tensile, pure shear, and mixed-mode) but not the true shear (Mode II) fracture for brittle materials. Thus, a new fracture criterion of maximum tension–shear SIF ratio is proposed [32] to judge both Mode I and Mode II fracture of single crack for brittle materials. The criterion judges whether the crack is the tensile or shear failure by the ratio of maximum SIF at 360° along the crack tip. It is promising to be applicable to multiple cracks.

In this work, the maximum Mode I and Mode II SIFs, $K_{I,k\max}(\theta)$ and $K_{II,k\max}(\theta)$ ($0^\circ < \theta < 360^\circ$), of inclined parallel multi-crack under uniaxial compression varying with the relative positions (including horizontal and vertical spacing) are calculated by the complex function and integration method to analyze their interacting mechanism, in order to determine strengthening and weakening zone of SIF. The initiation criterion of multi-crack is established based on the ratio of maximum tension–shear SIF for predicting the crack initiation (including initiation angle and load). Theoretical prediction results are verified by the uniaxial compression test of rock specimen with multi-crack.

2 Multiple cracks theory

2.1 SIF calculation formula of multiple cracks

Figure 1 shows an infinite plate of multiple cracks ($k=1, 2, \dots, K$) under uniform compressive and shear stresses at infinity (σ_x^∞ , σ_y^∞ and $\tau_{xy}^\infty = \tau_{yx}^\infty$, let the tensile stress be positive and the compressive stress be negative). It is assumed that all cracks are non-closed. Set a global rectangular coordinate system (xOy) and a local rectangular coordinate system ($x_kO_ky_k$) at the centers of the k th crack (O_k), where x axis is the horizontal direction and x_k axis is along the direction of the k th crack. Let a_k and α_k denote the half-length of the k th crack and the inclined angle with respect to the x axial. The anti-clockwise direction of α_k is defined to be positive.

For SIF calculation of multi-crack, the remote uniform stresses (σ_x^∞ , σ_y^∞ , $\tau_{xy}^\infty = \tau_{yx}^\infty$) applied to the infinite plate of multi-crack can be equivalent to the uniform surface stresses (p_k and q_k) applied to each crack (Fig. 1):

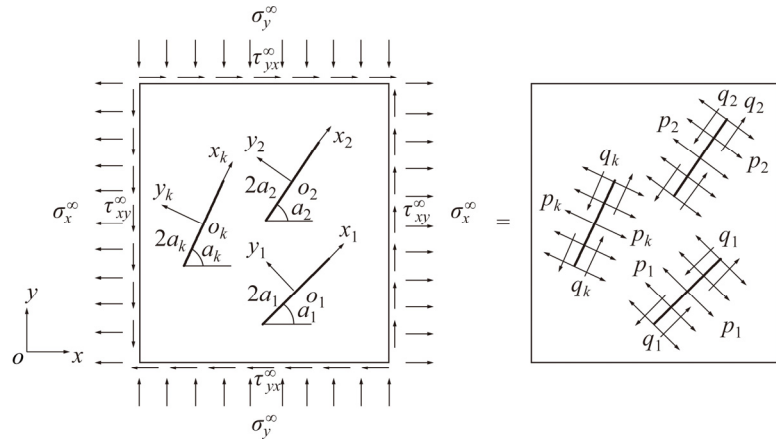


Fig. 1 Infinite plate containing k cracks

$$\begin{cases} p_k(s_k) = \frac{\sigma_x^\infty + \sigma_y^\infty}{2} + \frac{\sigma_y^\infty - \sigma_x^\infty}{2} \cos 2\alpha_k - \tau_{xy}^\infty \sin 2\alpha_k \\ q_k(s_k) = \frac{\sigma_x^\infty - \sigma_y^\infty}{2} \sin 2\alpha_k + \tau_{xy}^\infty \cos 2\alpha_k \end{cases} \quad (1)$$

The actual normal and tangential stresses (P_k, Q_k) existing on the surface of each crack are unknown, called as pseudo tractions [17,33]. The P_k and Q_k can be regarded as the integration of the two pairs of self-balancing surface forces (P, Q), as shown in Fig. 2. In order to investigate the multi-crack interaction, it needs to first determine the normal and tangential tractions (σ_y^c, τ_{xy}^c) of an arbitrary point $z (z=x+iy)$ in any direction (angle α), which is caused by two pairs of self-balancing surface forces (P, Q) at any point ($s, 0$) of a single crack, respectively.

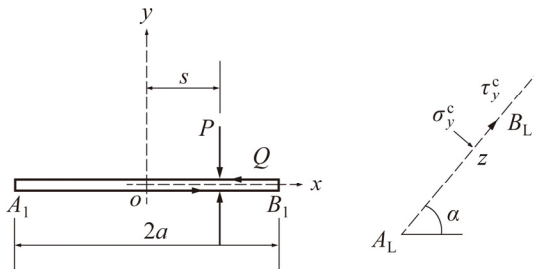


Fig. 2 Single crack under two pairs of self-balancing normal and tangential forces on crack surface

The stresses can be expressed in the form of the complex variable method as follows:

$$\begin{cases} \sigma_{xx} + \sigma_{yy} = 4\text{Re}\Phi(z) \\ \sigma_{yy} - i\tau_{xy} = \Phi(z) + \Omega(\bar{z}) + (z - \bar{z})\overline{\Phi'(z)} \end{cases} \quad (2)$$

The boundary condition is

$$\begin{cases} \sigma_{yy}^+ = \sigma_{yy}^- = P\delta(t-s) \quad (-a \leq t \leq a) \\ \sigma_{xy}^+ = \sigma_{xy}^- = Q\delta(t-s) \quad (-a \leq t \leq a) \end{cases} \quad (3)$$

According to Muskhelishvili plane elastic mechanics solution [24], there are

$$\begin{aligned} \sigma_y^c - i\tau_{xy}^c = & -\frac{P-iQ}{2\pi i} \sqrt{s^2 - a^2} [G(z) + e^{-2i\alpha} \overline{G(z)}] - \\ & \frac{P+iQ}{2\pi i} \sqrt{s^2 - a^2} [\overline{G(z)}(1 - e^{-2i\alpha}) + \\ & e^{-2i\alpha} (z - \bar{z})\overline{G'(z)}] \end{aligned} \quad (4)$$

where

$$\begin{aligned} G(z) &= \frac{1}{\sqrt{z^2 - a^2} (z - s)}, \\ G'(z) &= \frac{a^2 + sz - 2z^2}{(z^2 - a^2)^{3/2} (z - s)^2} \end{aligned} \quad (5)$$

When $P=1$ and $Q=0$, there is

$$\begin{aligned} \sigma_y^c - i\tau_{xy}^c = f_{nn} - if_{nt} = & -\frac{\sqrt{a^2 - s^2}}{2\pi} \\ & [G(z) + \overline{G(z)} + e^{-2i\alpha} (z - \bar{z})\overline{G'(z)}] \end{aligned} \quad (6)$$

where f_{nn} and f_{nt} indicate the normal and tangential tractions of any point z in any direction (angle α), caused by a pair of self-balancing unit normal forces ($P=1$) at any point ($s, 0$) on the crack surface, respectively.

When $P=0$ and $Q=1$, there is

$$\sigma_y^c - i\tau_{xy}^c = f_{in} - if_{it} = -\frac{\sqrt{a^2 - s^2}}{2\pi} [G(z)(1 - 2e^{-2i\alpha}) - G(z) + e^{-2i\alpha}(z - \bar{z})\overline{G'(z)}] \quad (7)$$

where f_{in} and f_{it} indicate the normal and tangential tractions of any point z in any direction (angle α), caused by a pair of self-balancing unit normal forces ($Q=1$) at any point $(s, 0)$ on the crack surface, respectively.

Considering the multi-crack interaction and superposition principle, the total normal and tangential stresses of any crack surface (k) are equal to the sum of $P_k(s_k)$ and $Q_k(s_k)$ acting on the k th crack itself and additional pseudo tractions caused by $P_l(s_l)$ and $Q_l(s_l)$ acting on the other crack surfaces ($l \neq k$). Therefore, the interacting surface normal and tangential stresses of any crack ($P_k(s_k)$ and $Q_k(s_k)$) can be calculated by solving the Fredholm integral equations [24]:

$$P_k(s_k) + \sum_{l=1, l \neq k}^L \int_{-a_l}^{a_l} P_l(s_l) f_{nm, lk}(s_l, s_k) ds_l + \sum_{l=1, l \neq k}^L \int_{-a_l}^{a_l} Q_l(s_l) f_{tn, lk}(s_l, s_k) ds_l = p_k(s_k) \quad (-a_k < s_k < a_k, k=1, 2, 3, \dots, K) \quad (8)$$

$$Q_k(s_k) + \sum_{l=1, l \neq k}^L \int_{-a_l}^{a_l} P_l(s_l) f_{nt, lk}(s_l, s_k) ds_l + \sum_{l=1, l \neq k}^L \int_{-a_l}^{a_l} Q_l(s_l) f_{tt, lk}(s_l, s_k) ds_l = q_k(s_k) \quad (-a_k < s_k < a_k, k=1, 2, 3, \dots, K) \quad (9)$$

where $p_k(s_k)$ and $q_k(s_k)$ are obtained by Eq. (1).

The kernel function f can be calculated by Eqs. (6) and (7). Its subscript has a clear physical meaning, e.g., $f_{nt, lk}(s_l, s_k)$ means the effect of unit normal force at a point $(s_l, 0)$ of the l th crack on the normal force at a point $(s_k, 0)$ of the k th crack.

Mode I and Mode II SIFs of any crack ($k=1, 2, \dots, K$) on its original plane ($\theta=0^\circ$) $K_{I,k}(0)$ and $K_{II,k}(0)$ can be determined by substituting $P_k(s_k)$ and $Q_k(s_k)$ into the following equations [24] and making calculation program by Mathematica software:

$$\begin{cases} K_{I,k}^\pm(0) = -\frac{1}{\sqrt{\pi a_k}} \int_{-a_k}^{a_k} P_k(s_k) \frac{a_k \pm s_k}{\sqrt{a_k^2 - s_k^2}} ds_k \\ K_{II,k}^\pm(0) = -\frac{1}{\sqrt{\pi a_k}} \int_{-a_k}^{a_k} Q_k(s_k) \frac{a_k \pm s_k}{\sqrt{a_k^2 - s_k^2}} ds_k \end{cases} \quad (10)$$

where the superscript “ \pm ” of K represents the left (+) and right (–) tips of the crack.

2.2 Initiation criterion of multiple cracks

For judging multi-crack initiation, it needs to calculate the interacting Mode I and Mode II SIFs of any crack ($k=1, 2, \dots, K$) in any direction ($0^\circ < \theta < 360^\circ$) based on the $K_{I,k}(0)$ and $K_{II,k}(0)$ on its original plane [32]:

$$\begin{cases} K_{I,k}(\theta_k) = K_{I,k}(0) \cos^3 \frac{\theta_k}{2} - 3K_{II,k}(0) \sin \frac{\theta_k}{2} \cos^2 \frac{\theta_k}{2} \\ K_{II,k}(\theta_k) = K_{I,k}(0) \sin \frac{\theta_k}{2} \cos^2 \frac{\theta_k}{2} + K_{II,k}(0) \cos \frac{\theta_k}{2} (1 - 3\sin^2 \frac{\theta_k}{2}) \end{cases} \quad (11)$$

According to

$$\begin{cases} \frac{\partial K_{I,k}(\theta_k)}{\partial \theta} = 0, \frac{\partial^2 K_{I,k}(\theta_k)}{\partial \theta^2} < 0 \\ \frac{\partial K_{II,k}(\theta_k)}{\partial \theta} = 0, \frac{\partial^2 K_{II,k}(\theta_k)}{\partial \theta^2} < 0 \end{cases} \quad (12)$$

The maximum values of $K_{I,k}(0)$ and $K_{II,k}(0)$ at θ_{IC} and θ_{IIC} , $K_{I,k \max}(\theta)$ and $K_{II,k \max}(\theta)$, can be obtained, respectively.

According to the criterion of maximum tension–shear SIF ratio for the single crack [32], the multi-crack initiation criterion can be established by substituting the interacting SIF of multi-crack:

$$\begin{cases} \frac{K_{I,k}(\theta_k)_{\max}}{K_{II,k}(\theta_k)_{\max}} > \frac{K_{IC}}{K_{IIC}}, K_{I,k}(\theta_k)_{\max} = K_{IC} \\ \text{at } \theta_{IC,k}, \text{ Mode I fracture} \\ \frac{K_{I,k}(\theta_k)_{\max}}{K_{II,k}(\theta_k)_{\max}} < \frac{K_{IC}}{K_{IIC}}, K_{II,k}(\theta_k)_{\max} = K_{IIC} \\ \text{at } \theta_{IIC,k}, \text{ Mode II fracture} \end{cases} \quad (13)$$

where K_{IC} and K_{IIC} are Mode I and Mode II fracture toughnesses, respectively.

3 Calculation of three parallel cracks under uniaxial compression

3.1 Calculation model of three parallel cracks

Take the infinite plate of three equal-length ($2a=30$ mm) parallel cracks ($\alpha=45^\circ$) under remote uniform compressive stress as the calculation

example. There are two cases for change of the horizontal and vertical spacings: (1) Fixing the lower crack A_1B_1 and the upper crack A_3B_3 , moving the middle crack A_2B_2 (which is equivalent to the case of fixing the middle crack A_2B_2 and moving the lower crack A_1B_1 and the upper crack A_3B_3); (2) Fixing the lower crack A_1B_1 and the middle crack A_2B_2 and moving the upper crack A_3B_3 (which is equivalent to the case of fixing the upper crack A_3B_3 and moving the lower crack A_1B_1 and the middle crack A_2B_2). Let D_s and D'_s denote the horizontal spacing (along the crack direction) of center-point connecting lines between A_2B_2 and A_1B_1 , A_3B_3 and A_1B_1 , respectively. Let D_h and D'_h denote the vertical spacing (perpendicular to the crack direction) of center-point connecting lines between A_2B_2 and A_1B_1 , A_3B_3 and A_1B_1 , respectively. Effects of crack relative positions on interacting SIF are analyzed as follows.

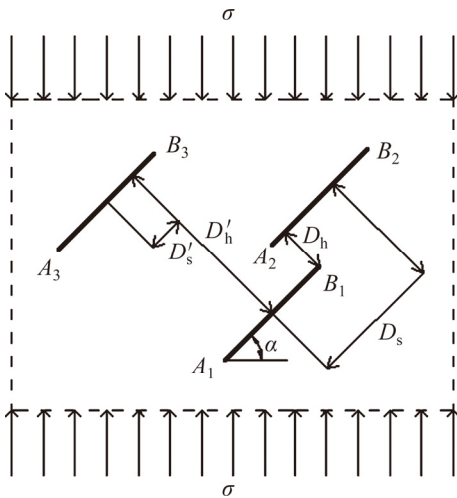


Fig. 3 Three parallel cracks

3.2 Effects of crack relative positions on interacting SIF

(1) Change of D_s

Let $D_h=20$ mm, $D'_h=40$ mm, $D'_s=0$ with only change of D_s (in term of D_s/a). Figure 4 illustrates the effects of D_s on the normalized Mode I and Mode II SIFs (in term of $K_{I,kmax}(\theta)/K_{I,max}^0(\theta)$ and $K_{II,kmax}(\theta)/K_{II,max}^0(\theta)$) of each crack-tip for multi-crack. $K_{I,kmax}(\theta)$ and $K_{II,kmax}(\theta)$ are the maximum values of $K_{I,k}(\theta)$ and $K_{II,k}(\theta)$ at θ_{IC} and θ_{IIC} . $K_{I,max}^0(\theta)$ and $K_{II,max}^0(\theta)$ are the maximum values of Mode I and Mode II SIFs of the single crack with the same length ($2a=30$ mm) and inclined angle ($\alpha=45^\circ$), and they can be determined by the calculation method in Ref. [32]. Define

$K_{I,kmax}(\theta)/K_{I,max}^0(\theta)<1$ (or $K_{II,kmax}(\theta)/K_{II,max}^0(\theta)<1$) as weakening-interaction, and $K_{I,kmax}(\theta)/K_{I,max}^0(\theta)>1$ (or $K_{II,kmax}(\theta)/K_{II,max}^0(\theta)>1$) as strengthening-interaction, and $K_{I,kmax}(\theta)/K_{I,max}^0(\theta)=1$ (or $K_{II,kmax}(\theta)/K_{II,max}^0(\theta)=1$) as non-interaction.

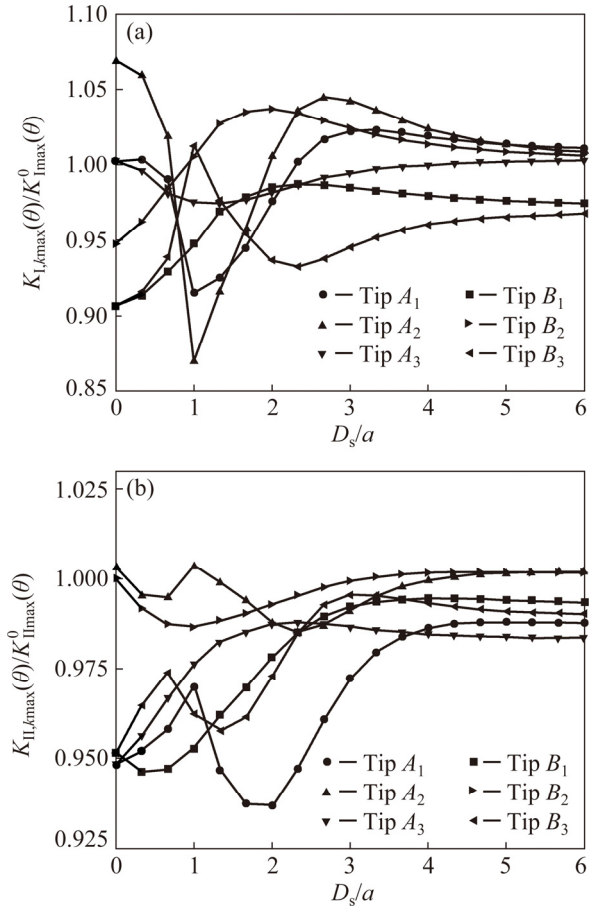


Fig. 4 Effects of horizontal spacing D_s on SIFs of all crack-tips: (a) $K_{I,kmax}(\theta)/K_{I,max}^0(\theta)$; (b) $K_{II,kmax}(\theta)/K_{II,max}^0(\theta)$

For the Mode I SIF, when D_s is 0 (central points of the three cracks are co-line), $K_{I,kmax}(\theta)/K_{I,max}^0(\theta)$ of points A_1 and A_3 is equal to 1 and $K_{I,kmax}(\theta)/K_{I,max}^0(\theta)$ of point A_2 is within 1.0–1.1, meaning that there is very few crack interaction. $K_{I,kmax}(\theta)/K_{I,max}^0(\theta)$ values of points A_1 , A_2 and A_3 are all decreased first when D_s/a is in the range of 0–1 (i.e., weakening-interaction of cracks is increased) and then increased for D_s/a larger than 1 (i.e., weakening-interaction of cracks is decreased). Finally, they tend to be stable values ($K_{I,kmax}(\theta)/K_{I,max}^0(\theta)=1$) when D_s/a becomes quite larger, i.e., the middle crack A_2B_2 is far away from the lower crack A_1B_1 and the upper crack A_3B_3 without any crack-interaction. Differently, $K_{I,kmax}(\theta)/K_{I,max}^0(\theta)$ of points B_1 , B_2 , and B_3 is less than 1 when D_s/a is 0 (with weakening effect). It increases when D_s/a is

less than 1 (i.e., weakening-interaction of cracks is decreased). Then, $K_{I,kmax}(\theta)/K_{IImax}^0(\theta)$ of points B_1 and B_2 increases and that of point B_3 decreases (i.e., weakening-interaction of cracks is increased) for D_s/a larger than 1. Finally, it also tends to be stable value ($K_{I,kmax}(\theta)/K_{IImax}^0(\theta) \approx 1$) when D_s/a becomes quite larger.

For the Mode II SIF, $K_{II,kmax}(\theta)/K_{IIImax}^0(\theta)$ values of all crack tips are nearly unchanged as D_s increases ($K_{II,kmax}(\theta)/K_{IIImax}^0(\theta) = 0.9-1$). Furthermore, two crack-tips of each crack (A_1 and B_1 , A_2 and B_2 , A_3 and B_3) have almost the same values of $K_{II,kmax}(\theta)/K_{IIImax}^0(\theta)$, because the moving of the middle crack A_2B_2 along the crack direction (i.e., the direction of shear stress) has little effect on the shear stress field. In addition, $K_{II,kmax}(\theta)/K_{IIImax}^0(\theta)$ of points A_1 and A_3 is slightly smaller than 1 and that of point A_2 is larger than 1 when D_s is 1. Therefore, the effect of D_s on Mode II SIFs of all crack tips could be neglected.

To sum up, when D_s changes, the strengthening zones of SIFs appear when the horizontal spacings are $D_s/a = 2.3-4.3$ for the bottom crack (A_1B_1), $D_s/a = 1-4$ for the middle crack (A_2B_2), and $D_s/a = 0.3-1$ for the upper crack (A_3B_3), respectively. $K_{I,kmax}(\theta)/K_{IImax}^0(\theta)$ values of points A_1 , A_2 and A_3 are minimum when D_s/a is 1 (i.e., $D_s/(2a) = 0.5$) and $K_{I,kmax}(\theta)/K_{IImax}^0(\theta)$ values of points B_1 , B_2 and B_3 have peak values when D_s/a is 2. This means that $K_{I,kmax}(\theta)/K_{IImax}^0(\theta)$ of all crack-tips reaches its maximum or minimum value when the horizontal spacing (D_s) is equal to times of half crack-length.

(2) Change of D'_s

Let $D_h = 20$ mm, $D'_h = 40$ mm and $D_s = 0$ with only change of D'_s (in term of D'_s/a). Figure 5 illustrates the effects of D'_s on the normalized Mode I and Mode II SIFs (in term of $K_{I,kmax}(\theta)/K_{IImax}^0(\theta)$ and $K_{II,kmax}(\theta)/K_{IIImax}^0(\theta)$) of each crack-tip.

For the Mode I SIF, $K_{I,kmax}(\theta)/K_{IImax}^0(\theta)$ values of points A_1 , A_2 and A_3 are nearly equal to 1 when D'_s is 0, indicating that there is almost no crack-interaction. When D'_s/a is in the range of 0–0.3, $K_{I,kmax}(\theta)/K_{IImax}^0(\theta)$ values of points A_1 , A_2 and A_3 all increase (i.e., strengthening-interaction of cracks is increased), and they decrease when D'_s/a is in the range of 0.3–1. $K_{I,kmax}(\theta)/K_{IImax}^0(\theta)$ of points A_1 and A_3 increases and that of point A_2 decreases for D'_s/a larger than 1. Finally, the value tends to be stable ($K_{I,kmax}(\theta)/K_{IImax}^0(\theta) = 1$) when D'_s/a becomes

quite larger, i.e., the upper crack A_3B_3 is far away from both the lower crack A_1B_1 and the middle crack A_2B_2 without any crack-interaction. Differently, $K_{I,kmax}(\theta)/K_{IImax}^0(\theta)$ values of points B_1 , B_2 and B_3 are less than 1 (with weakening effect) when D'_s is 0. They all increase when D'_s/a is in the range of 0–1 (i.e., weakening-interaction of cracks is decreased). $K_{I,kmax}(\theta)/K_{IImax}^0(\theta)$ of points B_1 and B_3 increases and that of point B_2 decreases (i.e., weakening-interaction of cracks is increased) for D'_s/a greater than 1. Finally, it also tends to be stable value ($K_{I,kmax}(\theta)/K_{IImax}^0(\theta) \approx 1$) when D'_s/a becomes quite larger.

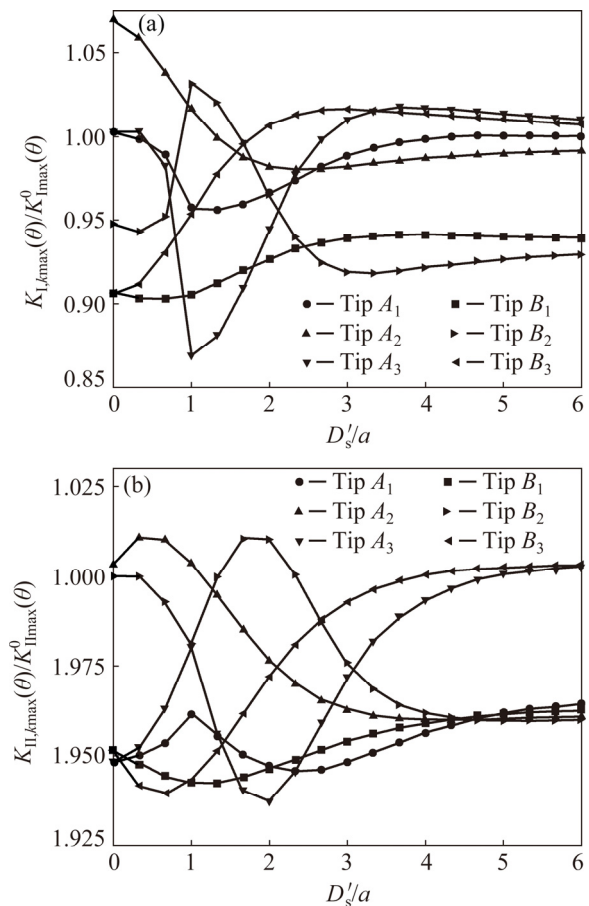


Fig. 5 Effects of horizontal spacing D'_s on SIFs of all crack-tips: (a) $K_{I,kmax}(\theta)/K_{IImax}^0(\theta)$; (b) $K_{II,kmax}(\theta)/K_{IIImax}^0(\theta)$

For the Mode II SIF, $K_{II,kmax}(\theta)/K_{IIImax}^0(\theta)$ values of all crack tips are nearly unchanged as D'_s increases ($K_{II,kmax}(\theta)/K_{IIImax}^0(\theta) = 0.9-1$). Furthermore, two crack-tips of each crack (A_1 and B_1 , A_2 and B_2 , A_3 and B_3) have almost the same values of $K_{II,kmax}(\theta)/K_{IIImax}^0(\theta)$, because the moving of the upper crack A_3B_3 along the crack direction (i.e., the direction of shear stress) has little effect on the shear stress field. In addition, $K_{II,kmax}(\theta)/K_{IIImax}^0(\theta)$ of

points B_1 , B_2 and B_3 is slightly less than 1 when D'_s is 0. $K_{II,kmax}(\theta)/K_{II,max}^0(\theta)$ of points B_1 and B_3 is slightly less than 1 and that of point B_2 is nearly equal to 1 when D'_s/a is 0.3. Therefore, the effect of D'_s on Mode II SIF of all crack tips could be neglected.

To sum up, $K_{I,kmax}(\theta)/K_{I,max}^0(\theta)$ and $K_{II,kmax}(\theta)/K_{II,max}^0(\theta)$ of each crack always have a peak point when D'_s/a is 1. By comparing Fig. 4 with Fig. 5, it is easy to find that the values of $K_{II,kmax}(\theta)$ of all cracks are all less than those of $K_{I,kmax}(\theta)$ whether the upper crack A_3B_3 moves or the middle crack A_2B_2 moves. It is indicated that Mode II fracture is hard to occur when the horizontal spacing (along the crack direction) of cracks varies.

(3) Change of D_h

Let $D_s=0$, $D'_s=0$, $D'_h=40$ mm with only change of D_h (in term of D_h/a). Figure 6 illustrates the effects of D_h on the normalized Mode I and Mode II SIFs of each crack-tip.

For the Mode I SIF, all of the crack-tips A_1 , A_2 , A_3 and B_1 , B_2 , B_3 have similar tendencies with the

change of D_h , since the three central points of the three cracks are always colinear and the effects on the two-tips of each crack are almost the same. Differently, $K_{I,kmax}(\theta)/K_{I,max}^0(\theta)$ values of points A_1 , A_2 , A_3 are always larger than 1 (i.e., strengthening-interaction) while those of points B_1 , B_2 , B_3 are always less than 1 (i.e., weakening-interaction). When D_h/a is less than -5 , $K_{I,kmax}(\theta)/K_{I,max}^0(\theta)$ values of all crack tips tend to be stable, since the middle crack A_2B_2 is far away from the lower crack A_1B_1 . When D_h/a is in the range from -5 to -1 , they all increase, and when D_h/a varies from -1 to 0 , they all decrease, because the middle crack A_2B_2 is gradually close to the lower crack A_1B_1 . When D_h/a increases from 0 to 1 , $K_{I,kmax}(\theta)/K_{I,max}^0(\theta)$ values of points A_1 , A_2 , A_3 and B_3 increase while those of points B_1 and B_2 decrease. When D_h/a is in the range of $1-2$, $K_{I,kmax}(\theta)/K_{I,max}^0(\theta)$ values of points A_1 , A_2 , B_1 and B_2 increase while those of points A_3 and B_3 decrease. When D_h/a increases from 2 to 3 , $K_{I,kmax}(\theta)/K_{I,max}^0(\theta)$ values of points A_1 , A_3 , B_1 and B_3 increase while those of points A_2 and B_2 decrease, because A_2B_2 begins to keep away from A_1B_1 and close to A_3B_3 . $K_{I,kmax}(\theta)/K_{I,max}^0(\theta)$ values of all crack-tips also tend to be stable for D_h/a greater than 3 , since the middle crack A_2B_2 is far away from the upper crack A_3B_3 .

For the Mode II SIF, $K_{II,kmax}(\theta)/K_{II,max}^0(\theta)$ of cracks A_1B_1 and A_2B_2 nearly have the same fluctuation characteristics as $K_{I,kmax}(\theta)/K_{I,max}^0(\theta)$, but the crack A_3B_3 has different fluctuation characteristics of $K_{II,kmax}(\theta)/K_{II,max}^0(\theta)$. They all tend to be stable when D_h/a becomes quite larger. Furthermore, two crack-tips of each crack (A_1 and B_1 , A_2 and B_2 , A_3 and B_3) have almost the same values of $K_{II,kmax}(\theta)/K_{II,max}^0(\theta)$.

To sum up, when D_h changes, strengthening zones of SIFs appear when the vertical spacings (D_h/a) are in the range from -4 to -1 for the bottom (A_1B_1) and upper cracks (A_3B_3), and from -5 to -1 for the middle (A_2B_2) crack. Thus, the strengthening zone is from -4 to -1 for all cracks. When D_h/a is equal to 1 or -1 , the SIFs of the crack tips have the peak values. $K_{I,kmax}(\theta)/K_{I,max}^0(\theta)$ and $K_{II,kmax}(\theta)/K_{II,max}^0(\theta)$ of both the cracks A_2B_2 and A_3B_3 reach the peak values (i.e., dangerous case) at $D_h/a=2$ and $D_h/a=3$, respectively, i.e., the interacting of multi-crack is the strongest when the vertical spacing is equal to times of half crack-length. The study of the strongest interacting zone is of great significance

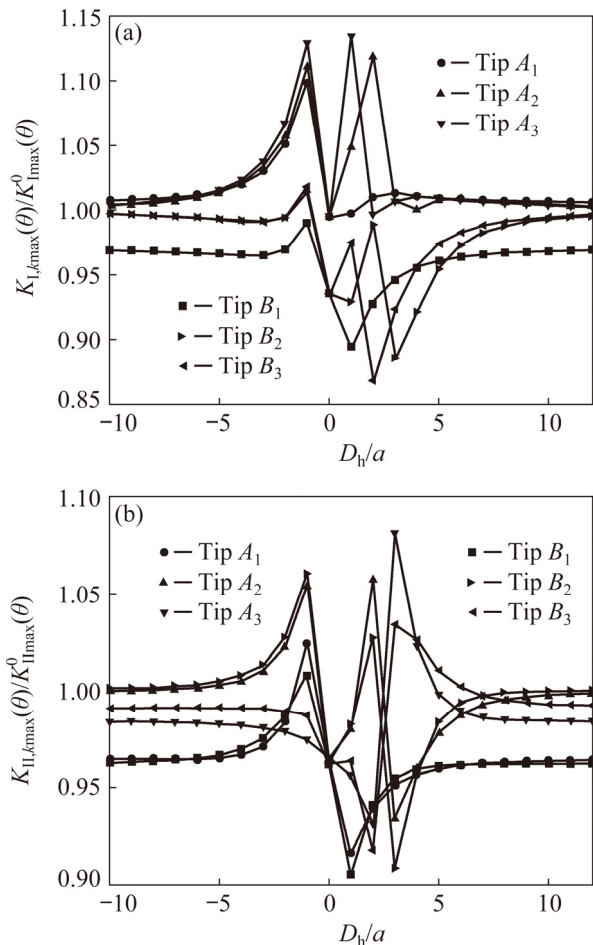


Fig. 6 Effects of vertical spacing D_h on SIFs of all crack-tips: (a) $K_{I,kmax}(\theta)/K_{I,max}^0(\theta)$; (b) $K_{II,kmax}(\theta)/K_{II,max}^0(\theta)$

for cracking arrest in engineering.

(4) Change of D'_h

Let $D_s=0$, $D'_s=0$, $D_h=20$ mm with only change of D'_h (in term of D'_h/a). Figure 7 illustrates the effects of D'_h on the normalized Mode I and Mode II SIFs of each crack-tip.

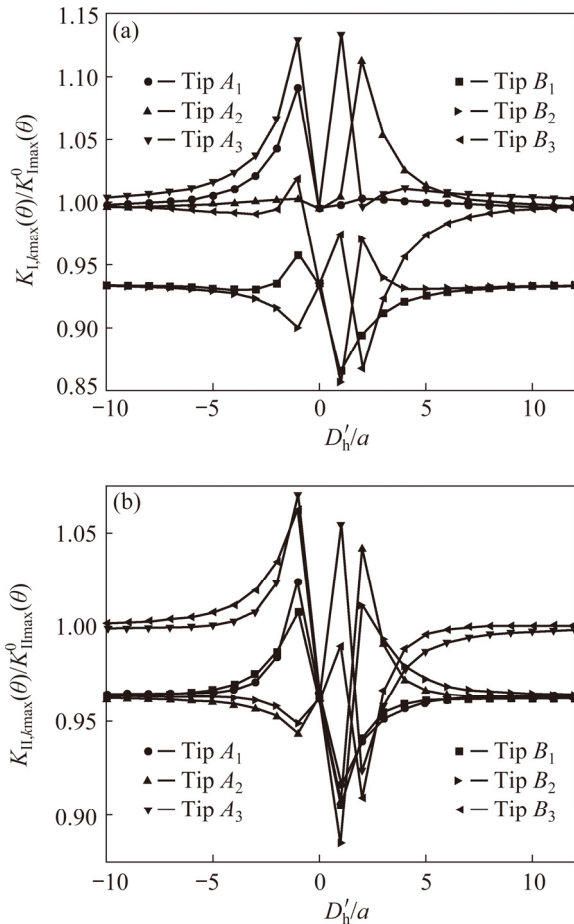


Fig. 7 Effects of vertical spacing D'_h on SIFs of all crack-tips: (a) $K_{I,kmax}(\theta)/K_{I,max}^0(\theta)$; (b) $K_{II,kmax}(\theta)/K_{II,max}^0(\theta)$

For the Mode I SIF, all of the crack-tips A_1 , A_2 , A_3 , B_1 , B_2 and B_3 almost have similar tendencies with change of D'_h . Differently, $K_{I,kmax}(\theta)/K_{I,max}^0(\theta)$ values of points A_1 , A_2 and A_3 are always larger than 1 (i.e., strengthening-interaction) while those of points B_1 , B_2 and B_3 are always less than 1 (i.e., weakening-interaction). When D'_h/a is less than -4 , $K_{I,kmax}(\theta)/K_{I,max}^0(\theta)$ values of all crack tips tend to be stable, since the upper crack A_3B_3 is far away from the lower crack A_1B_1 . When D'_h/a is in the range from -4 to -1 , $K_{I,kmax}(\theta)/K_{I,max}^0(\theta)$ of point B_2 decreases while that of all other points increases. When D'_h/a varies from -1 to 0 , $K_{I,kmax}(\theta)/K_{I,max}^0(\theta)$ of point B_2 increases while that of all other points

decreases. When D'_h/a increases from 0 to 1, $K_{I,kmax}(\theta)/K_{I,max}^0(\theta)$ values of points A_1 , A_2 , A_3 and B_3 increase while those of points B_1 and B_2 decrease. When D'_h/a is in the range from 1 to 2, $K_{I,kmax}(\theta)/K_{I,max}^0(\theta)$ values of points A_1 , A_2 , B_1 and B_2 increase while those of points A_3 and B_3 decrease. This is because when D'_h/a varies from -4 to 0 , the upper crack A_3B_3 is gradually close to the lower crack A_1B_1 and the middle crack A_2B_2 . When D'_h/a is 0, the crack A_3B_3 coincides with the crack A_1B_1 ; when D'_h/a is in the range of $0-2$, A_3B_3 begins to keep away from A_1B_1 and close to A_2B_2 . $K_{I,kmax}(\theta)/K_{I,max}^0(\theta)$ values of all crack-tips tend to be stable for D'_h/a larger than 2.

For the Mode II SIF, the cracks A_1B_1 and A_3B_3 have the same fluctuation characteristics of $K_{II,kmax}(\theta)/K_{II,max}^0(\theta)$ as those of $K_{I,kmax}(\theta)/K_{I,max}^0(\theta)$, but the crack A_2B_2 has different fluctuation characteristics of $K_{II,kmax}(\theta)/K_{II,max}^0(\theta)$. They all tend to be stable when D'_h/a becomes quite larger. Furthermore, two crack-tips of each crack have almost the same values of $K_{II,kmax}(\theta)/K_{II,max}^0(\theta)$.

To sum up, when D'_h changes, strengthening zones of SIFs appear when the vertical spacings (D'_h/a) are from -3 to -1 for the bottom crack (A_1B_1), from -3 to 2 for the middle crack (A_2B_2) and from -4 to 1 for the upper crack (A_3B_3). Thus, the strengthening zone of all cracks is D'_h/a from -3 to -1 . Therefore, the vertical spacing of multi-crack is better not to be times of half crack-length for crack-arrest. In addition, the values of $K_{I,kmax}(\theta)$ are always larger than those of $K_{II,kmax}(\theta)$ and therefore the tensile (Mode I) fracture is more likely to occur than the shear (Mode II) fracture. When D'_h/a or D'_h/a tends to zero (i.e., two cracks would coincide with each other), the value of SIF fluctuates greatly. It is indicated that the change of the multi-crack number would result in the fluctuation of SIF.

Figure 8 shows calculation results of $K_{II}(0)$ compared with those in Refs. [23,34]. They agree very well (with an error of less than 5%), indicating that Eq. (10) is valid and feasible.

3.3 Initiation prediction of three parallel cracks

For predicting the initiation parameters of the three equal-length ($2a=20$ mm) parallel cracks ($\alpha=45^\circ$) in the infinite plate under remote uniform compressive stresses, red sandstone was adopted as rock material and its basic mechanical parameters

are listed in Table 1, including compressive strength σ_c , tensile strength σ_t , elastic modulus E , Mode I and Mode II fracture toughness K_{IC} and K_{IIC} .

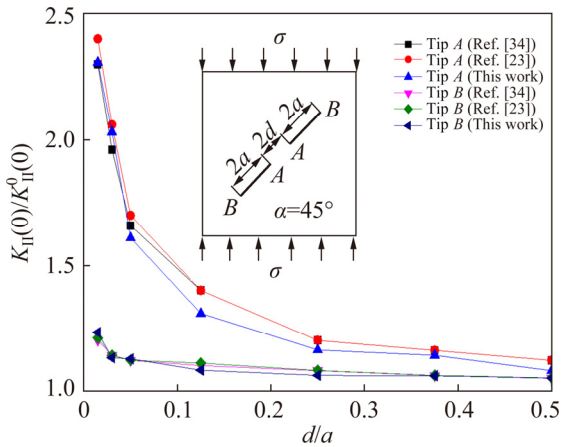


Fig. 8 Normalized $K_{II}(0)$ versus d/a

Table 1 Mechanical parameters of red sandstone

σ_t / MPa	σ_c / MPa	φ / (°)	E / GPa	K_{IC} / (MPa·m ^{1/2})	K_{IIC} / (MPa·m ^{1/2})
3.75	65	33.5	9.08	0.47	1.22

Based on the analytic results (i.e., the interaction among cracks is related to times of half crack-length), two groups of three-crack relative position parameters were selected for predicting initiation (Table 2). In the first group, D'_s ($D'_s=0$), D_h ($D_h=15$ mm), and D'_h ($D'_h=30$ mm) are unchanged and D_s is equal to times of half crack-length ($a=10$ mm). In the second group, D_s ($D_s=0$), D'_s ($D'_s=0$) and D'_h ($D'_h=30$ mm) are unchanged and D_h is equal to times of half crack-length ($a=10$ mm).

Table 2 Relative positions of three parallel cracks ($D'_s=0$, $D'_h=30$ mm, $\alpha=45^\circ$)

Group	Specimen	D_s /mm	D_h /mm
1	1	0	15
	2	10	
	3	20	
	4	30	
	5	40	
2	1	0	-20
	2		-10
	3		10
	4		20
	5		30

Take Specimen 1 in Group 1 as an example for illustrating how to predict the crack initiation. Firstly, Mode I and Mode II SIFs of each crack-tip were calculated by Eq. (10), and these SIFs were substituted into Eq. (13) to obtain the initiation load, initiation angle, and fracture mechanism of each crack-tip. And then, the actual initiation tip (A_2) can be determined according to the minimum initiation load of the crack-tip (Table 3). The prediction results of all specimens are listed in Table 4. It is seen that the initiation load is changed less with the increase of the D_s/a and the initiation mechanism of multi-crack is Mode I.

Table 3 Prediction results of initiation parameters of Specimen 1 in Group 1

Crack tip	Tip initiation load/MPa	Initiation angle/(°)	Fracture mode
A_1	30.75	-128.09	Mode I
B_1	32.35	-125.81	Mode I
A_2	28.58	-128.29	Mode I
B_2	30.60	-125.68	Mode I
A_3	30.75	-128.08	Mode I
B_3	32.34	-125.81	Mode I

Table 4 Prediction results of multi-crack initiation parameters

Group No.	Specimen No.	Initiation load/MPa	Initiation tip	Initiation angle/(°)	Fracture mode
1	1	28.58	A_2	-128.29	Mode I
	2	30.29	A_2	-127.3	Mode I
	3	29.52	B_2	-52.00	Mode I
	4	29.30	B_2	52.53	Mode I
	5	29.29	A_2	52.54	Mode I
2	1	28.14	A_2	-125.98	Mode I
	2	26.35	A_2	-122.31	Mode I
	3	29.58	A_2	-128.62	Mode I
	4	27.41	A_2	-124.54	Mode I
	5	29.86	A_2	52.73	Mode I

4 Test verification

4.1 Test arrangement

The red sandstone from Wuding County, Chuxiong city of Yunnan province, China, was chosen as rock material. Its basic mechanical parameters are given in Table 1.

The DNS100 electro-hydraulic servo universal testing machine (Fig. 9(a)) was adopted for the uniaxial compression test with a maximum loading force of 1000 kN. The displacement loading rate was 0.1 mm/s. During the tests, stress–strain curves of all specimens were recorded for determining the crack initiation load. After the tests, fracture trajectories of all specimens were analyzed to obtain the multi-crack initiation angle. Figure 9(b) shows a cuboid specimen (100 mm × 100 mm × 20 mm) with three equal-length ($2a=20$ mm) parallel cracks ($\alpha=45^\circ$). The relative positions of the three cracks are given in Table 2.

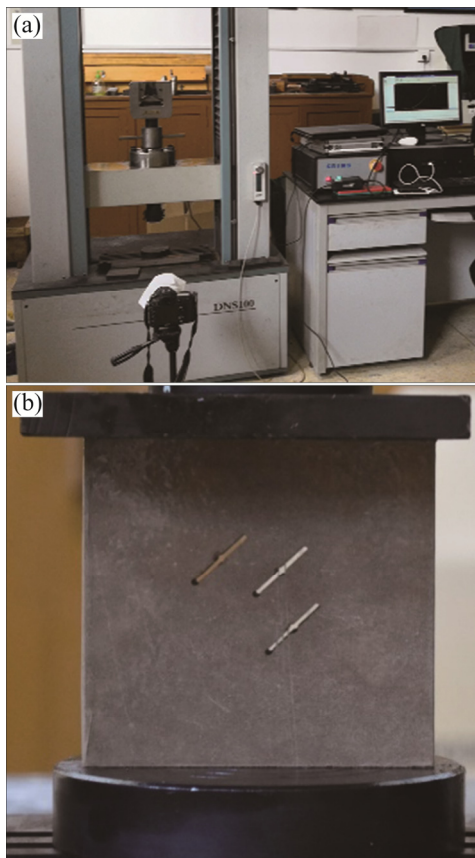


Fig. 9 Uniaxial compression test: (a) Test machine; (b) Loading status

4.2 Results and analysis

Figure 10 shows the stress–strain curve of Specimen 1 as an example. It is divided into four stages (which is consistent with Refs. [35,36]): initial compaction (OA , where the slope is gradually increased), linear elastic deformation (AB , where the slope is constant), nonlinear deformation (BC , where the slope is gradually decreased) and post-peak failure (CD). The crack initiation load can be determined by the distinguishing point (B) of linear

elastic deformation and nonlinear deformation.

Fracture trajectories of the red sandstone specimens are shown in Figs. 11 and 12. It can be found that the cracks first initiate at one crack tip, then propagate stably, and finally link up until failure. For example, the tip A_2 of Specimen 1 initiates first, and then tips A_1 , B_1 , B_2 and B_3 begin to initiate. After that, the tips A_2 and B_3 are connected and finally the tips A_1 and B_2 are connected until failure. It is worth noting that the initiation of the secondary crack is accompanied by the propagation of main cracks, due to the redistribution of crack-tip stress caused by the initiation of the wing crack.

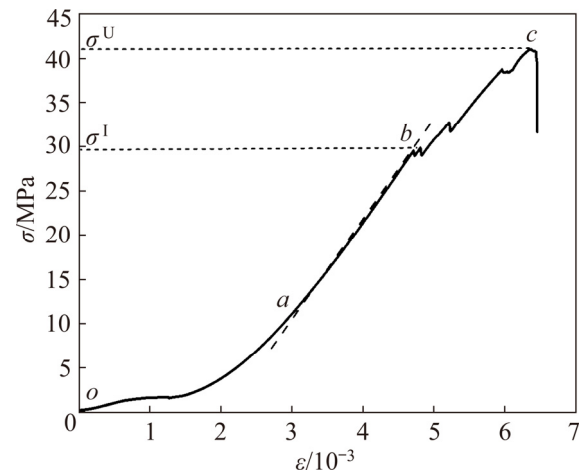


Fig. 10 Stress–strain curve of Specimen 1

Table 5 lists the test results of crack initiation parameters for all specimens. The fracture mechanism of all red sandstone specimens in uniaxial compressive is tensile (Mode I) fracture. By comparing Table 5 with Table 4, it can be concluded that the test results are in good agreement with the prediction results, which can verify the validity of the interacting mechanism and the multi-crack initiation criterion.

According to the displacement results of the finite element method, the initial open crack is still open under compression before the crack initiates ($\mu=0$). Take Specimen 1 in Group 1 (100 mm × 100 mm × 20 mm) with three equal-length parallel cracks (length $2a=20$ mm and width $t=1.5$ mm) as example. Figure 13 shows nephogram of y -direction displacement (δ_y) at the peak stress $\sigma^U=40.97$ MPa, where DMX and SMN are the maximum and minimum displacement. Table 6 lists δ_y and its projected displacement (δ_i) onto vertical direction

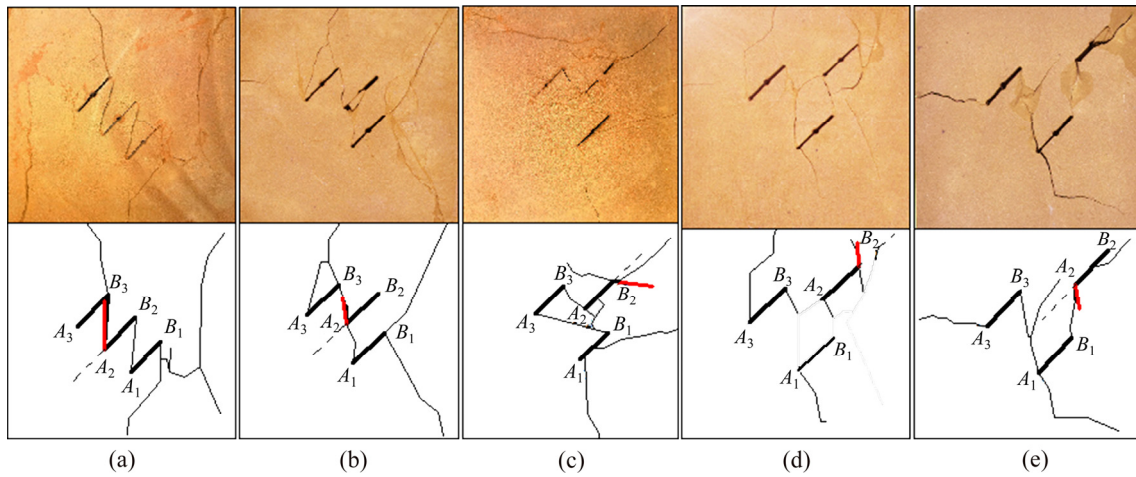


Fig. 11 Fracture trajectories of red sandstone specimens with different D_s : (a) $D_s/a=0$; (b) $D_s/a=1$; (c) $D_s/a=2$; (d) $D_s/a=3$; (e) $D_s/a=4$

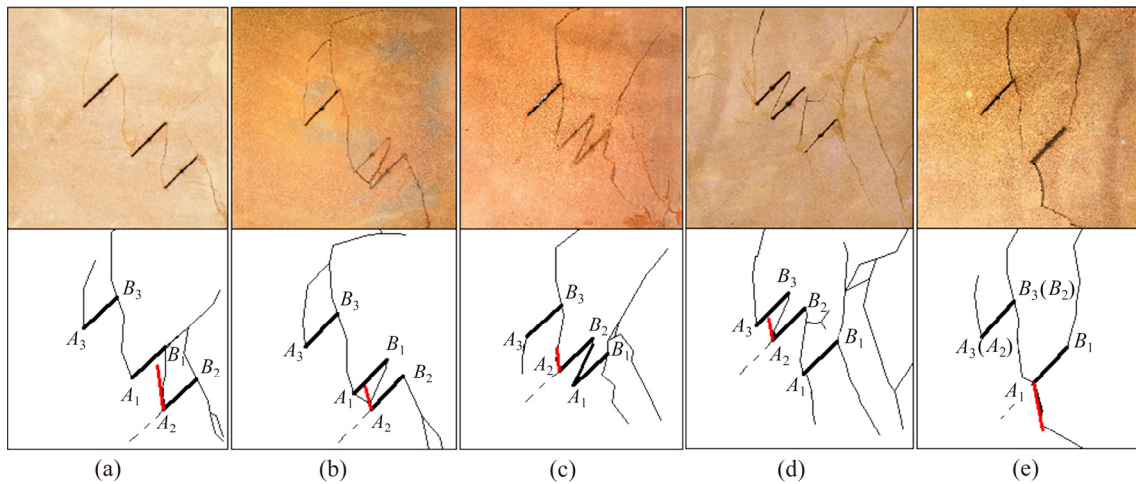


Fig. 12 Fracture trajectories of red sandstone specimens with different D_h : (a) $D_h/a=-2$; (b) $D_h/a=-1$; (c) $D_h/a=1$; (d) $D_h/a=2$; (e) $D_h/a=3$

Table 5 Test results of crack initiation parameters for all specimens

Group	Specimen No.	Initiation load/MPa	Initiation tip	Initiation angle/(°)	Fracture Mode
1	1	28.52	A_2	-133	Mode I
	2	29.24	A_2	-133	Mode I
	3	28.17	B_2	-51	Mode I
	4	32.15	B_2	49.5	Mode I
	5	28.25	A_2	50	Mode I
2	1	24.35	A_2	-128	Mode I
	2	27.303	A_2	-127	Mode I
	3	30.595	A_2	-117	Mode I
	4	27.365	A_2	-129	Mode I
	5	31.125	A_2	55	Mode I

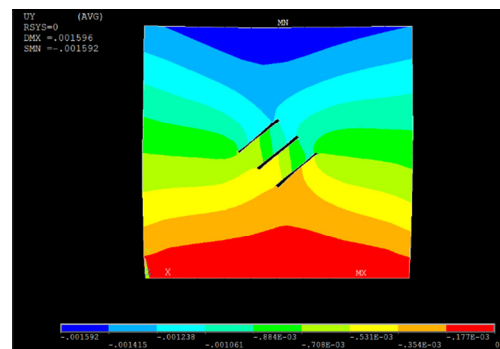


Fig. 13 Nephogram of y -direction displacement

of the original crack ($\delta_i = \delta_y \sin 45^\circ$) of each crack tip. It can be seen that all $\delta_i \leq t$, indicating that the initial crack is still open before the crack initiates. Similar results can be also obtained from other rock specimens.

Table 6 Displacement of each crack tip

Crack tip	Tip No.	δ_y/mm	δ_r/mm
A_1	1	-0.377	-0.267
	2	-0.296	-0.209
B_1	3	-0.820	-0.580
	4	-0.681	-0.482
A_2	5	-0.536	-0.379
	6	-0.438	-0.310
B_2	7	-1.03	-0.729
	8	-0.929	-0.657
A_3	9	-0.779	-0.551
	10	-0.642	-0.454
B_3	11	-1.18	-0.838
	12	-1.09	-0.776

5 Conclusions

(1) The maximum Mode I and Mode II SIFs $K_{I,k\max}(\theta)$ and $K_{II,k\max}(\theta)$ ($0^\circ < \theta < 360^\circ$) of the inclined parallel multi-crack under uniaxial compression varying with the relative positions (including horizontal and vertical spacing) are calculated by the complex function and integration method to analyze their interacting mechanism. The accuracy of this method is validated by comparing the test results obtained with the approximate method and the Kachanov method.

(2) The multi-crack initiation criterion is established based on the ratio of maximum tension–shear SIF in order to predict the multi-crack initiation angle, load, and mechanism. It can provide a theoretical basis for safety assessment and crack-arrest design in rock mass engineering.

(3) The horizontal and vertical spacings have greater effect on $K_{I,k\max}(\theta)$ than on $K_{II,k\max}(\theta)$. The SIF strengthening zones of all cracks appear only when the vertical spacings are D_h/a from -4 to -1 and D'_h/a from -3 to -1. It is better not to let the vertical spacing of multi-crack equal to times of half crack-length for avoiding the strengthening zone and possible fracture. The initiation load changes less with the increase of the D_s/a and the initiation mechanism of multi-crack is Mode I.

(4) The test results of the red-sandstone cube specimens with three parallel cracks under uniaxial compression agree well with the prediction results and can prove the validity of the multi-crack initiation criterion.

Acknowledgments

The authors are grateful for the financial supports from the National Natural Science Foundation of China (51874351, 51474251), Hunan Provincial Innovation Foundation For Postgraduate, China (CX2018B047), the Open Sharing Fund for the Large-scale Instruments and Equipments of Central South University, China (CSUZC201923).

References

- [1] XU Jun, ZHENG Zhe-yuan, XIAO Xiao-chun, LI Zhao-xia. Crack propagation and coalescence due to dual non-penetrating surface flaws and their effect on the strength of rock-like material [J]. Journal of Geophysics and Engineering, 2018, 15: 938–951.
- [2] YANG Sheng-qi. Crack coalescence behavior of brittle sandstone samples containing two coplanar fissures in the process of deformation failure [J]. Engineering Fracture Mechanics, 2011, 78: 3059–3081.
- [3] YANG Sheng-qi, TIAN Wen-ling, HUANG Yan-hua, RANJITH P G, JU Yang. An experimental and numerical study on cracking behavior of brittle sandstone containing two non-coplanar fissures under uniaxial compression [J]. Rock Mechanics and Rock Engineering, 2016, 49: 1497–1515.
- [4] CAO Ping, CAO Ri-hong, ZHAO Yan-lin, ZHANG Ke, PU Cheng-zhi, FAN Wen-cheng. Propagation-coalescence and rheologic fracture behavior of rock cracks [J]. The Chinese Journal of Nonferrous Metals, 2016, 26: 1737–1762. (in Chinese)
- [5] ZHAO Yan-lin, WAN Wen, WANG Wei-jun, WANG Min, PENG Qing-yang. Fracture experiments on ordered multi-crack body in rock-like materials under uniaxial compression and numerical simulation of wing cracks [J]. Chinese Journal of Geotechnical Engineering, 2013, 35: 2097–2109. (in Chinese)
- [6] YANG Xu-xu, JING Hong-wen, TANG Chun-an, YANG Sheng-qi. Effect of parallel joint interaction on mechanical behavior of jointed rock mass models [J]. International Journal of Rock Mechanics and Mining Sciences, 2017, 92: 40–53.
- [7] SAGONG M, BOBET A. Coalescence of multiple flaws in a rock-model material in uniaxial compression [J]. International Journal of Rock Mechanics and Mining Sciences, 2002, 39: 229–241.
- [8] CHEN Miao, YANG Sheng-qi, GAMAGE R P, YANG Wen-dong, YIN Peng-fei, ZHANG Yuan-chao, ZHANG Qiang-yong. Fracture processes of rock-like specimens containing nonpersistent fissures under uniaxial compression [J]. Energies, 2019, 12: 79.
- [9] WONG L N Y, EINSTEIN H H. Crack coalescence in molded gypsum and carrara marble: Part 1. Macroscopic observations and interpretation [J]. Rock Mechanics and Rock Engineering, 2009a, 42: 475–511.
- [10] WONG L N Y, EINSTEIN H H. Crack coalescence in molded gypsum and carrara marble: Part 2. Microscopic observations and interpretation [J]. Rock Mechanics and Rock Engineering, 2009b, 42: 513–545.
- [11] XIAO Tao-li, LI Xin-ping, JIA Shan-po. Failure characteristics of rock with two pre-existing transfixion

- cracks under triaxial compression [J]. Chinese Journal of Rock Mechanics and Engineering, 2015, 34: 2455–2462. (in Chinese)
- [12] WANG Y H, THAM L G, LEE P K K, TSUI Y. A boundary collection method for cracked plates [J]. Computers and Structures, 2003, 81(28–29): 2621–2630.
- [13] KOBAYASHI A S, CHEREPY R D, KINSEL W C. A numerical procedure for estimating the stress intensity factor of a crack in a finite plate [J]. Journal of Fluids Engineering, 1964, 86: 681–684.
- [14] CHEUNG Y K, WOO C W, WANG Y H. The stress intensity factor for a double edge cracked plate by boundary collocation method [J]. International Journal of Fracture, 1988, 37: 217–231.
- [15] BENTHEM J P, KOITER W T. Asymptotic approximations to crack problems [M]. Leyden: Springer, Dordrecht, 1973: 131–178.
- [16] SNEDDON I N, LOWENGRUB M. Crack problems in the classical theory of elasticity [M]. New York: Wiley, 1969: 713–751.
- [17] HORII H, NEMAT-NASSER S. Compression-induced microcrack growth in brittle solids: Axial splitting and shear failure [J]. Journal of Geophysical Research, 1985, 90: 3105–3125.
- [18] HORII H, NEMAT-NASSER S. Elastic fields of interacting inhomogeneities [J]. International Journal of Solids and Structures, 1985, 21: 731–745.
- [19] KACHANOV M. Effective elastic properties of cracked solids: Critical review of some basic concepts [J]. Applied Mechanics Reviews, 1992, 45: 304–335.
- [20] KACHANOV M. Elastic solids with many cracks: A simple method of analysis [J]. International Journal of Solids and Structures, 1987, 23: 23–43.
- [21] KACHANOV M. A simple technique of stress analysis in elastic solids with many cracks [J]. International Journal of Fracture, 1985, 28: 11–19.
- [22] ZHU Di-jie, CHEN Zhong-hui, XI Jing-yi, YANG Deng-feng. Interaction between offset parallel cracks in rock [J]. Chinese Journal of Geotechnical Engineering, 2017, 39: 235–243. (in Chinese)
- [23] LI Yin-ping, THAM L G, WANG Yuan-han, TSUI Y. A modified Kachanov method for analysis of solids with multiple cracks [J]. Engineering Fracture Mechanics, 2003, 70: 1115–1129.
- [24] CHEUNG Y K, WOO C W, WANG Y H. A general method for multiple crack problems in a finite plate [J]. Computational Mechanics, 1992, 10: 335–343.
- [25] ERDOGAN F, SIH G C. On the crack extension in plates under plane loading and transverse shear [J]. Journal of Basic Engineering, 1963, 85: 519–527.
- [26] MAITI S K, SMITH R A. Comparison of the criteria for mixed mode brittle fracture based on the preinstability of stress-strain field. Part II: Pure shear and uniaxial compressive loading [J]. International Journal of Fracture, 1984, 24: 5–22.
- [27] YU Mao-hong. Twin shear stress yield criterion [J]. International Journal of Mechanical Sciences, 1983, 25: 71–74.
- [28] CHANG K J. On the maximum strain criterion—A new approach to the angled crack problem [J]. Engineering Fracture Mechanics, 1981, 14: 107–124.
- [29] SIH G C. Strain energy density factor applied to mixed mode crack problems [J]. International Journal of Fracture, 1974, 10: 305–321.
- [30] PALANISWAMY K, KNAUSS W G. Propagation of a crack under general in-plane tension [J]. International Journal of Fracture, 1972, 8: 114–117.
- [31] SHEN Bao-tang, STEPHANSSON O. Modification of the G-criterion for crack propagation subjected to compression [J]. Engineering Fracture Mechanics, 1994, 47: 177–189.
- [32] RAO Qiu-hua, SUN Zong-qi, STEPHANSSON O, LI Chun-lin, STILLBORG B. Shear fracture (Mode II) of brittle rock [J]. International Journal of Rock Mechanics and Mining Sciences, 2003, 40: 355–375.
- [33] DENG H, NEMAT-NASSER S. Microcrack interaction and shear fault failure [J]. International Journal of Damage Mechanics, 1994, 3: 3–37.
- [34] CHEN Yi-zhou. General case of multiple crack problems in an infinite plate [J]. Engineering Fracture Mechanics, 1984, 20: 591–598.
- [35] LI Zhuo, RAO Qiu-hua, LI Peng, YI Wei. Crack initiation rate of brittle rock under thermal-hydro-mechanical coupling condition [J]. Transactions of Nonferrous Metals Society of China, 2018, 28: 2107–2113.
- [36] YI Wei, RAO Qiu-hua, LI Zhuo, SHEN Qing-qing. A new measurement method of crack propagation rate for brittle rock under THMC coupling condition [J]. Transactions of Nonferrous Metals Society of China, 2019, 29: 1728–1736.

多裂纹相互作用机理及起裂预测

沈晴晴, 饶秋华, 李卓, 易威, 孙栋良

中南大学 土木工程学院, 长沙 410075

摘要: 采用复变函数和积分方法, 计算多条平行斜裂纹的最大 I 型和 II 型应力强度因子 $K_{I,kmax}(\theta)$ 和 $K_{II,kmax}(\theta)$ ($0^\circ < \theta < 360^\circ$) 随裂纹相对位置(包括垂直间距和水平间距)的变化值, 分析多裂纹相互作用机理, 并得到应力强度因子的强化区和弱化区。基于最大拉-剪应力强度因子比, 建立多裂纹起裂判据, 并预测裂纹起裂角、起裂荷载和起裂机理。预测结果表明: 多裂纹起裂机理为 I 型; 为便于止裂, 多裂纹之间的垂直间距不宜等于裂纹半长的倍数。预测结果与单轴压缩下三平行裂纹的红砂岩立方体试件试验结果吻合较好, 验证多裂纹起裂准则的有效性。

关键词: 相互作用机理; 多裂纹起裂判据; 起裂预测; 多裂纹; 应力强度因子

(Edited by Bing YANG)